Inorganic Chemistry

Article

pubs.acs.org/IC

Host–Guest Supramolecular Interactions in the Coordination Compounds of 4,4′-Azobis(pyridine) with MnX_2 (X = NCS^-, $NCNCN^-$, and PF_6^-): Structural Analyses and Theoretical Study

Paramita Kar,[†] Rituparna Biswas,[†] Michael G. B. Drew,[‡] Antonio Frontera,*[,§] and Ashutosh Ghosh*[,†]

[†]Department of Chemistry, University College of Science, University of Calcutta, 92, APC Road, Kolkata-700 009, India

[‡]School of Chemistry, The University of Reading, P.O. Box 224, Whiteknights, Reading RG6 6AD, U.K.

[§]Departament de Química, Universitat de les Illes Balears, Crta. de Valldemossa km 7.5, 07122 Palma de Mallorca, Baleares, Spain

Supporting Information

ABSTRACT: Three new Mn(II) coordination compounds $\{[Mn(NCNCN)_2(azpy)]\cdot 0.5azpy\}_n$ (**1**), $\{[Mn(NCS)_2(azpy)(CH_3OH)_2]\cdot azpy\}_n$ (**2**), and $[Mn(azpy)_2(H_2O)_4][Mn(azpy)(H_2O)_5]\cdot 4PF_6\cdot H_2O\cdot 5.5azpy$ (**3**) (where azpy = 4,4′-azobis(pyridine)) have been synthesized by self-assembly of the primary ligands, dicyanamide, thiocyanate, and hexafluorophosphate, respectively, together with azpy as the secondary spacer. All three complexes were characterized by elemental analyses, IR spectroscopy, thermal analyses, and single crystal X-ray crystallography. The structural analyses reveal that complex **1** forms a two-dimensional (2D) grid sheet motif. These sheets assemble to form a microporous framework that incorporates coordination-free azpy by host–guest $\pi\cdots\pi$ and C–H···N hydrogen bonding interactions. Complex **2** features azpy bridged one-dimensional (1D) chains of centrosymmetric $[Mn(NCS)_2(CH_3OH)_2]$ units which form a 2D porous sheet via a $CH_3\cdots\pi$ supramolecular interaction. A guest azpy molecule is incorporated within the pores by strong H-bonding interactions. Complex **3** affords a 0-D motif with two monomeric Mn(II) units in the asymmetric unit. There exist $\pi\cdots\pi$, anion$\cdots\pi$, and strong hydrogen bonding interactions between the azpy, water, and the anions. Density functional theory (DFT) calculations, at the M06/6-31+G* level of theory, are used to characterize a great variety of interactions that explicitly show the importance of host–guest supramolecular interactions for the stabilization of coordination compounds and creation of the fascinating three-dimensional (3D) architecture of the title compounds.

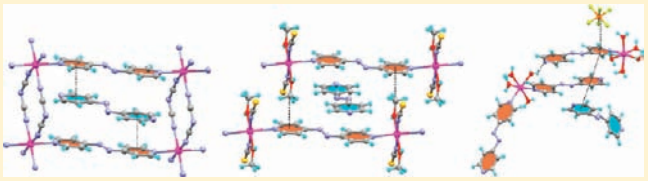

INTRODUCTION

Porous coordination polymers (PCPs) and metal organic frameworks (MOFs) have attracted tremendous interest in crystal engineering[1] not only because of their importance in the fundamental study of novel phenomena occurring in nanometer sized confined space,[2] but also for their potential applications in various fields such as storage,[3] separation,[4] catalysis,[5,6] and molecular arrays.[7,8] In porous compounds, guest molecules present within the channels or cavities are almost always connected by supramolecular contacts such as hydrogen bonds and aromatic interactions which contribute strongly to the formation of host–guest assemblies as well as dynamic frameworks.[9] It is well-known that guest molecules, which act as template units for the construction of porous materials, must be readily removable for pore creation to be useful in various applications.[10] However, some frameworks that have been prepared in the presence of a specific guest via supramolecular self-assembly processes have been found to collapse upon releasing of the guest to afford reversible systems.[11] The formation and stability of inclusion compounds depend on the magnitude and directions of intermolecular forces in the host–guest assembly. Single crystal X-ray analysis gives information about topology and packing of the molecules in the solid state, which is crucial for thermal stability and kinetics of formation and decomposition of such materials.[12]

Although supramolecular hydrogen bonding interactions are frequently used in the creation of frameworks and host–guest assemblies,[13] examples of systems that exploit aromatic interactions (e.g., $\pi\cdots\pi$, CH$\cdots\pi$, anion$\cdots\pi$, etc.) are relatively limited.[14] Computational methods are sometimes helpful for steering molecular assembly into prescribed crystal architectures based on well-defined structure directing interactions, such as hydrogen bonding, metal coordination, or aromatic interactions which can transcend the cumulative effect of the multitude of weaker forces, such as van der Waals interactions. Therefore, the quantitative knowledge of these interactions between host framework and guest molecules and also between the host frameworks are of considerable importance for the further development of molecular porous networks.

Polydentate ligands with pyridine groups or nitrogen-containing heterocycles, which are generally used as building blocks in the design of coordination frameworks, are capable of forming significant $\pi\cdots\pi$ interactions because of their electron poor ring systems. Moreover, the coordination of the nitrogen

Received: October 1, 2011
Published: January 24, 2012

   dx.doi.org/10.1021/ic202129a | *Inorg. Chem.* 2012, 51, 1837–1851

Table 1. Crystal Data and Structure Refinement of Complexes 1, 2, and 3

	1	2	3
formula	$C_{19}H_{12}MnN_{12}$	$C_{24}H_{24}MnN_{10}O_2S_2$	$C_{87}H_{88}F_{24}Mn_2N_{34}O_{10}P_4$
formula weight	436.35	603.59	2435.65
space group	$P\bar{1}$	$P2_1/c$	$P\bar{1}$
crystal system	triclinic	monoclinic	triclinic
a/Å	7.454(4)	7.241(5)	10.961(5)
b/Å	12.280(5)	16.985(5)	14.261(5)
c/Å	12.905(5)	12.010(5)	35.488(5)
α/deg	64.89(4)	(90)	83.934(5)
β/deg	83.52(4)	94.077(5)	84.808(5)
γ/deg	88.19(4)	(90)	89.492(5)
V/Å^3	1062.6(9)	1473.4(13)	5494(3)
Z	2	2	2
D_{calc}/g cm^{-3}	1.448	1.361	1.472
μ/mm^{-1}	(MoKα) 0.655	(MoKα) 0.629	(MoKα) 0.398
F(000)	470	622	2480
crystal size (mm)	0.08 × 0.08 × 0.24	0.07 × 0.09 × 0.15	0.06 × 0.09 × 0.11
θ range (deg)	2.8 to 30.0	2.1 to 35.7	0.6 to 24.8
R(int)	0.039	0.037	0.035
no of data measured	7451	25962	38034
no. of unique data	5936	6680	18607
data with $I > 2\sigma(I)$	4363	3699	11631
$R1$,$wR2$ for data $I > 2\sigma(I)$	0.0725, 0.1895	0.0471, 0.1468	0.0960, 0.2644
R1, wR2 for all data	0.0928, 0.2028	0.0985, 0.1468	0.1407, 0.3025
final electron density e/A^3	1.564, −1.396	0.723, 0.444	1.769, −0.856

atom of such ligands to a metal ion further enhances its electron withdrawing effect and makes them even more suited to form $\pi\cdots\pi$ interactions. The 4,4′-azobis(pyridine) (azpy) ligand is well-suited for the construction of supramolecular assemblies based on aromatic interactions because of its molecular planarity provided by the π-conjugated system and π-orbitals. In most of the previously reported coordination polymers of this ligand, the uncoordinated azpy usually occupies the pores or channels of the MOF aided by various types of weak noncovalent interactions with the coordinated azpy ligands or aromatic guests.[15] Indeed, the X-ray structures of the complexes allowed the identification and analyses of these interactions. However, theoretical investigations based on density functional theory (DFT) calculations are very useful for quantitative estimation of these types of supramolecular interactions and also for rationalization the experimental findings.

To realize the pivotal role of noncovalent interactions in supramolecular aggregates of azpy ligand, we have synthesized three complexes $\{[Mn(NCNCN)_2(azpy)]\cdot 0.5azpy\}_n$ (**1**), $\{[Mn(NCS)_2(azpy)(CH_3OH)_2]\cdot azpy\}_n$ (**2**), and $[Mn(azpy)_2(H_2O)_4][Mn(azpy)(H_2O)_5]\cdot 4PF_6\cdot H_2O\cdot 5.5azpy$ (**3**), and these are characterized by single crystal X-ray structures, IR spectroscopy, and thermal analyses. The structures of the complexes reveal that complex **1** features a two-dimensional (2D) microporous framework with the azpy guest in the pores held by host−guest $\pi\cdots\pi$ and C−H···N hydrogen bonding interactions. Complex **2** forms one-dimensional (1D) chains of $[Mn(NCS)_2(CH_3OH)_2]$ units bridged by the azpy ligand which undergoes $CH_3\cdots\pi$ interactions to form a 2D porous sheet. The azpy guest molecules are accommodated in the pores with the help of O−H···N H-bonding interactions. By sharp contrast, complex **3** affords a 0-D motif with two monomeric Mn(II) units where the uncoordinated azpy molecules are held by $\pi\cdots\pi$, anion$\cdots\pi$, and strong hydrogen bonding interactions. Weak forces play an important role in the construction of final three-dimensional (3D) polymeric structures in all the three complexes. Using DFT calculations on large fragments of the crystal structures, we have analyzed the great variety of interactions in the three complexes and how they influence self-assembly and host−guest binding motifs.

EXPERIMENTAL SECTION

Materials. The reagents and solvents used were of commercially available reagent quality unless otherwise stated and were used without further purification.

Synthesis of the Ligand. The 4,4′-azobis(pyridine) (azpy) was prepared as an orange solid following the literature method[16] by using 4-cyanopyridine and sodium hypochlorite.

Caution! *Perchlorate salts of metal complexes with organic ligands are potentially explosive. Only small amounts of material should be prepared and handled with great care.*

Synthesis of $\{[Mn(NCNCN)_2(azpy)]\cdot 0.5azpy\}_n$ (1). A solution of $Mn(ClO_4)_2\cdot 6H_2O$ (0.722 g, 2 mmol) in methanol (5 mL) was added to a solution of azpy (3 mmol, 0.552 g) in methanol (10 mL) followed by the addition of aqueous solution (10 mL) of Na(NCNCN) (4 mmol, 0.356 g). The resulting solution was stirred for about half an hour. The solution was then filtered to remove a small amount of orange precipitate, and the dark orange filtrate was left at room temperature. Orange plate-like single crystals suitable for X-ray diffraction (XRD) were obtained by slow evaporation of the mother liquor for several days. Yield was 71% (0.62 g) based on $Mn(ClO_4)_2\cdot 6H_2O$; Anal. Calcd for $C_{19}H_{12}MnN_{12}$: C, 49.25; H, 2.61; N, 36.28. Found: C, 49.22; H, 2.50; N, 36.20. IR (KBr pellet, cm^{-1}):2303, 2215, and 2178 ν_{s+as}(C═N), 1593 ν(N═N).

Synthesis of $\{[Mn(NCS)_2(azpy)(CH_3OH)_2]\cdot azpy\}_n$ (2). A solution of $Mn(ClO_4)_2\cdot 6H_2O$ (0.722 g, 2 mmol) in methanol (5 mL) was added to a solution of azpy (4 mmol, 0.736 g) in methanol (10 mL) followed by the addition of aqueous solution (10 mL) of NH_4SCN (4 mmol, 0.152 g). The resulting solution was stirred for about half an hour and then filtered to remove a small amount of orange precipitate. The dark orange filtrate was left at room temperature. Deep-orange single crystals suitable for XRD were obtained after a few days of

dx.doi.org/10.1021/ic202129a | Inorg. Chem. 2012, 51, 1837−1851

storage of the filtrate. Yield was 76% (0.92 g) based on $Mn(ClO_4)_2{\cdot}6H_2O$; Anal. Calcd for $C_{24}H_{24}MnN_{10}O_2S_2$: C, 47.76; H, 4.01; N, 23.21. Found: C, 47.70; H, 3.97; N, 23.15: IR (KBr pellet, cm^{-1}): 2062 ν(NCS),1593 ν(N═N), and 3036 $\nu(CH_3OH)$.

Synthesis of $[Mn(azpy)_2(H_2O)_4][Mn(azpy)(H_2O)_5]{\cdot}4PF_6{\cdot}H_2O{\cdot}5.5azpy$ (3). A solution of $Mn(ClO_4)_2{\cdot}6H_2O$ (0.361 g, 1 mmol) in methanol (5 mL) was added to a solution of azpy (5 mmol, 0.920 g) in methanol (10 mL) followed by the addition of aqueous solution (10 mL) of NH_4PF_6 (2 mmol, 0.326 g). The resulting solution was refluxed for about 1 h. The solution was then filtered, and the orange colored filtrate was kept undisturbed for several days. Deep-orange single crystals suitable for XRD were obtained from the solution. Yield was 73% (0.89 g) based on $Mn(ClO_4)_2{\cdot}6H_2O$; Anal. Calcd for $C_{87}H_{88}F_{24}Mn_2N_{32}O_{10}P_4$: C, 42.48; H, 3.61; N, 19.36. Found: C, 42.45; H, 3.59; N, 19.32 IR (KBr pellet, cm^{-1}): 3104 ν_{broad}(OH), 841 $\nu(PF_6^-)$, and 1593 ν(N═N).

Physical Measurements. Elemental analyses (C, H, and N) were performed using a 2400 series II CHN analyzer. IR spectra in KBr (4500−500 cm^{-1}) were recorded using a Perkin-Elmer RXI FT-IR spectrophotometer. Electronic spectra in the solid state (1000−250 nm) were recorded in a Hitachi U-3501 spectrophotometer. Thermal analyses (TG-DTA) were carried out on a Mettler Toledo TGA/SDTA 851 thermal analyzer in a dynamic atmosphere of dinitrogen (flow rate 30 cm^3min^{-1}). The samples were heated in an alumina crucible at a rate of 10 °C min^{-1}.

Crystallographic Data Collection and Refinement. Intensity data for complex **1** were collected with Mo Kα radiation at 150(2) K using the Oxford Diffraction X-Calibur CCD System. The crystals were positioned at 50 mm from the CCD. A total of 321 frames were measured with a counting time of 10 s. Data analysis was carried out with the CrysAlis program.[17] Suitable single crystals of complexes **2** and **3** were mounted on a Bruker SMART diffractometer equipped with a graphite monochromator and Mo−Kα (λ = 0.71073 Å) radiation. The crystals were positioned at 60 mm from the CCD. A total of 360 frames were measured with a counting time of 10 s. All three structures were solved using direct methods with the Shelxs97 program.[18]The non-hydrogen atoms were refined with anisotropic thermal parameters. The hydrogen atoms bonded to carbon were included in geometric positions and given thermal parameters equivalent to 1.2 times those of the atom to which they were attached. Absorption corrections were carried out for **1** using the ABSPACK program.[19] and for **2** and **3** using the SADABS program.[17] Data collection and structure refinement parameters and crystallographic data for the three complexes are given in Table 1.

Theoretical Methods. The present theoretical study has been carried out using DFT calculations by means of the Gaussian-09 package.[20] The level of theory is M06/6-31+G* for geometries and energies, which is an adequate compromise between the accuracy of the results and the size of the systems studied herein. The M06 functional is one of the most successful functionals for general applications and in particular for noncovalent interactions in chemical systems.[21] In all Mn complexes studied, the spin contamination is very small, even in the systems with four Mn ions, which shows the reliability of the level of theory and specially of the ability of the M06 functional to deal with transition metals. The binding energies were calculated with correction for the basis set superposition error (BSSE) by using the Boys−Bernardi counterpoise technique.[22]

RESULTS AND DISCUSSION

Syntheses. The complexes were obtained in high yield by allowing the azpy ligand to react with $Mn(ClO_4)_2{\cdot}6H_2O$ in a methanol solution followed by the addition of aqueous solution of Na(NCNCN) (for **1**), NH_4SCN (for **2**), or NH_4PF_6 (for **3**) in stoichiometric molar ratios. It is interesting to note that, during the synthesis of **1**, an increase in molar ratios (from 2:3 to 1:2 or higher) of Mn:azpy results in the formation of another complex $\{[Mn(NCNCN)(azpy)_2(H_2O)_2]ClO_4{\cdot}azpy{\cdot}(H_2O)_2\}_n$ as reported by Liao et al.[23] On the other hand, the solvent, not the Mn:azpy ratios plays the prominent role in the synthesis of compound **2**. For its synthesis, the solvent must be methanol−water mixture; if the same reaction is carried out in ethanol−water or in water, a different compound, $\{[Mn(NCS)_2(azpy)_2]{\cdot}azpy\}_n$[15a] as reported by Noro et al., resulted, irrespective of whether the Mn:azpy ratio was 1:1 or 1:2. The $CH_3{\cdots}\pi$ interactions between the coordinated methanol and the azpy ligand (see structure description and theoretical calculations) seems to be very important in the stabilization of compound **2**. The composition of compound **3** which is not a coordination polymer, depends neither on the Mn:azpy ratios nor on the reaction medium as it is obtained as the sole product in all cases even when the Mn:azpy ratio was varied in the range 1:1 to 1:5 in $MeOH/H_2O$ or $EtOH/H_2O$ medium.

Scheme 1. Schematic Representation for the Formation of Complexes 1−3

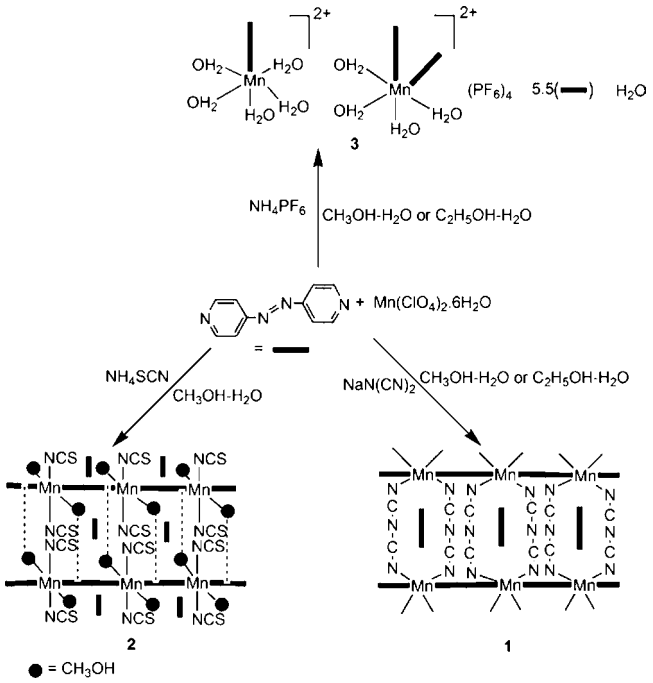

IR Spectra of the Complexes. Spectroscopic data and their assignments are given in the Experimental Section. The dicyanamide anion in Na(NCNCN) showed three sharp and strong characteristic bands in the frequency region 2290−2170 cm^{-1} which are attributed to ν_{asym} + ν_{sym} (C≡N) combination modes (2286 cm^{-1}), ν_{asym} (C≡N) (2232 cm^{-1}) and ν_{sym} (C≡N) (2179 cm^{-1}).[24] Upon complexation these bands shift toward higher frequencies. For compound **1**, the split bands at 2303, 2215, and 2178 cm^{-1} respectively can be attributed to the ν_{sym} + ν_{asym} (C≡N), ν_{asym} (C≡N), and ν_{sym} (C≡N) modes of the bridging dicyanamide ligand in the structure. Whereas for complex **2**, one sharp and strong band at 2062 cm^{-1} indicates the presence of the N bonded NCS^- group. Along with this, the appearance of a broad band at 3036 cm^{-1} indicates the presence of solvent methanol in this complex. In complex **3**, a broad band at 3104 cm^{-1} and a sharp peak at 841 cm^{-1} can be assigned to the characteristic stretching modes of water and hexafluorophosphate anion, respectively. In the region, expected for the N═N stretch vibration, compounds **1**, **2**, and **3** exhibit one single, sharp, and strong band at 1593 cm^{-1},

dx.doi.org/10.1021/ic202129a | Inorg. Chem. 2012, 51, 1837−1851

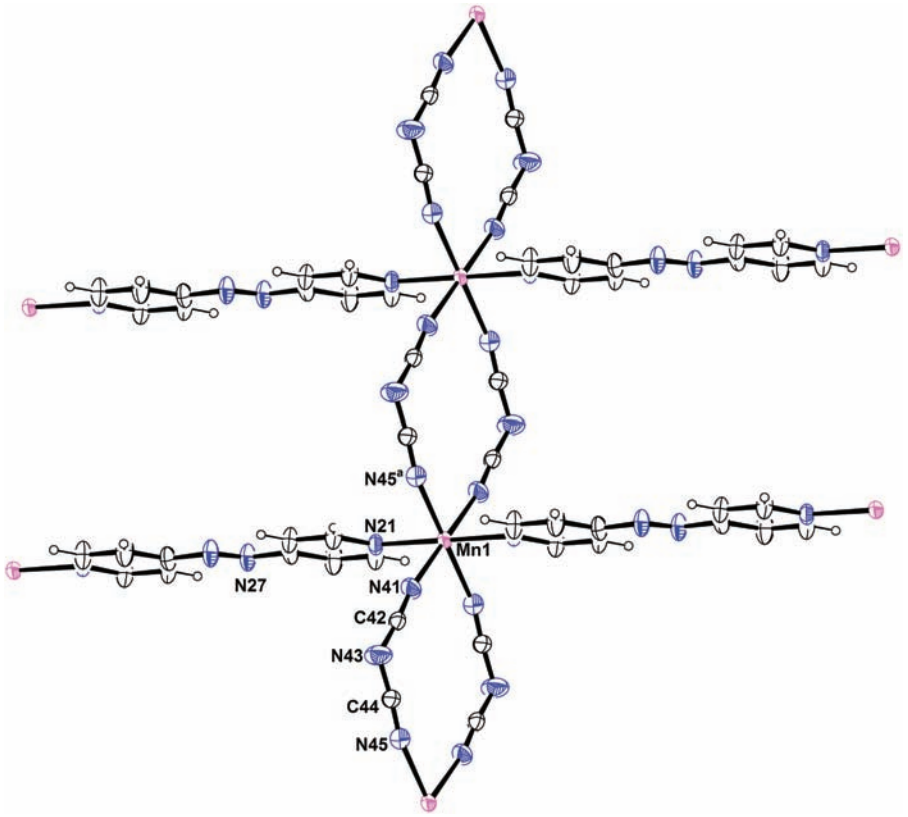

Figure 1. Structure of the discrete 2-dimensional polymeric unit around Mn(1) with ellipsoids at 30% probability. The superscript [a] represents symmetry code 1+*x*, *y*, *z*.

Table 2. Bond Distances (Å) and Angles (deg) in the Metal Coordination Spheres of Complex 1

atom labels	distance	atom labels	angle
Mn(1)–N(41)	2.219(3)	N(41)–Mn(1)–N(45)[a]	89.40(10)
Mn(1)–N(45)[a]	2.219(3)	N(21)–Mn(1)–N(45)[a]	90.55(10)
Mn(1)–N(21)	2.273(3)	N(41)– Mn(1)–N(21)	88.71(10)
Mn(2)–N(51)	2.195(3)	N(51)–Mn(2)–N(11)	91.79(10)
Mn(2)–N(55)[a]	2.207(3)	N(51)–Mn(2)–N(55)[a]	87.99(10)
Mn(2)–N(11)	2.287(3)	N(11)–Mn(2)–N(55)[a]	90.33(10)

[a]Symmetry code = 1+*x*, *y*, *z*.

attributable to the presence of the azpy moiety in all the structures.

Thermal Analyses. The thermogravimetric analyses were carried out in air on powder samples of **1**–**3**. In **1**, the first endothermic weight loss of 19.70%, corresponding to the departure of a half guest azpy molecule per asymmetric unit (calcd 19.85%), was observed between 220 and 275 °C (Supporting Information, Figure S1). The coordinated azpy ligand is held more strongly and, consequently, the second endothermic weight loss of 39.65% observed at higher temperature (between 290 and 340 °C) is attributable to the loss of coordinated azpy (calcd 39.71%). After removal of its guest azpy molecule at 275 °C, the isolated solid is dissolved in methanol, and the crystalline product obtained on slow evaporation of solvent is found to be identical to compound **1**. For compound **2**, the first endothermic weight loss of 10.53% (calcd 10.60%) between 110 and 130 °C corresponds to the departure of two molecules of coordinated methanol per formula unit. In the second step, between 160 and 230 °C an endothermic weight loss of 30.31% is observed which corresponds to the loss of one guest azpy per formula unit (calcd 30.48%). The TG curves (Supporting Information, Figure S2) indicate that the guest azpy ligand of **2** is lost at a lower temperature than in **1**. Interestingly, the solid isolated after removal of its guest azpy molecule reverts to compound **2** on crystallization from methanol but transforms into $\{[Mn(NCS)_2(azpy)_2]azpy\}_n$ on crystallization from ethanol. Therefore, it is clear that for the isolation of compound **2**, methanol plays an important role. The X-ray powder diffraction patterns of **1** and **2** differ considerably from those of the species isolated after the removal of the guest azpy molecule indicating that the supramolecular framework is not retained on removal of the guest molecules in both cases (Supporting Information, Figures S3 and S4). In compound **3**, the total weight loss of 67.12% (calcd 67.95%) was observed (Supporting Information, Figure S5) between 95 and 320 °C corresponding to the total loss of coordinated and uncoordinated water molecule and all the azpy ligands.

Description of Structures of Complexes 1, 2, and 3. The structure of **1** contains two discrete azpy and doubly dicyanamide bridged 2D polymers based on Mn(1) and Mn(2) respectively, both of which occupy centrosymmetric positions.

dx.doi.org/10.1021/ic202129a | *Inorg. Chem.* 2012, 51, 1837–1851

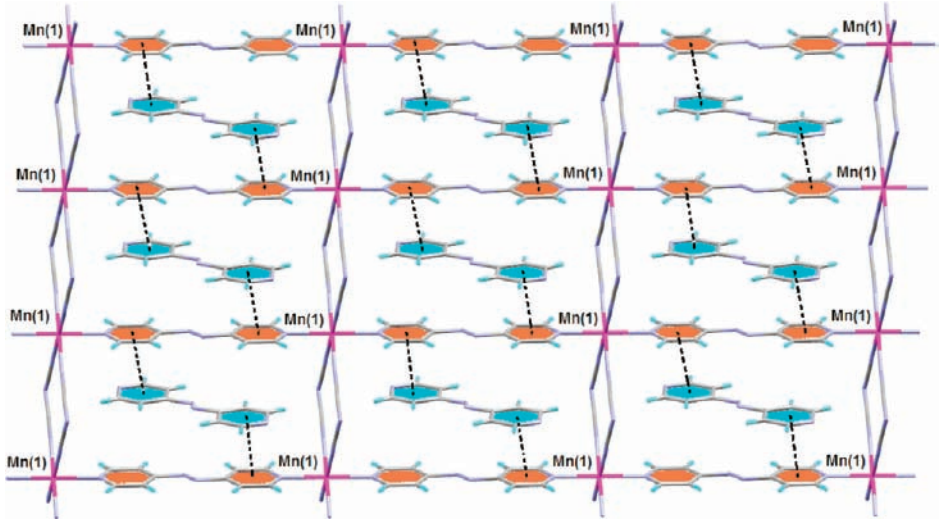

Figure 2. Formation of a 2D sheet involving $\pi\cdots\pi$ stacking interactions between host (orange) and guest (blue) azpy ligands.

In addition, for each $[Mn(NCNCN)_2(azpy)]_2$ moiety, there is one uncoordinated azpy which acts as a guest molecule. The structure of the polymer around Mn(1) is shown in Figure 1. That around Mn(2) is equivalent and is shown in the Supporting Information, Figure S6.

Each unit consists of octahedrally coordinated Mn(II) that is bonded to four nitrogen atoms of different N−C−N−C−N ligands together with two nitrogen atoms from azpy ligands. Bond lengths around the metal atoms are Mn(1)−N(41) 2.219(3) Å and Mn(1)−N(45)[a] (symmetry code [a] = 1+x, y, z) 2.219(3) Å to the NCNCN ligand and Mn(1)−N(21) 2.273(3) Å to the nitrogen of azpy. In the second polymeric system, bond lengths to the NCNCN ligand are slightly shorter with Mn(2)−N(51) 2.195(3) Å, Mn(2)−N(55) (1+x, y, z) 2.207(3) Å and Mn(2)−N(11) 2.287(3) Å. Selected bond lengths and angles are summarized in Table 2. The two pyridine rings of the azpy ligands are perforce coplanar. The terminal nitrogen atoms of each dicyanamide ion coordinates to symmetry related manganese ions with both Mn(1)···Mn(1) and Mn(2)···Mn(2) separations of 7.454 Å and thus forms a 12 membered ring. As a result of repetition of this 12 membered ring, an almost linear chain of $\mu_{1,5}$ dicyanamide-briged Mn(II) is formed along the a axis. Both doubly dicyanamide bridged Mn(II) centers are further connected by 4,4′-azpy linkers in the c direction to generate 2D sheets for both polymeric systems. The 2D sheets formed by Mn(1) are further stabilized by $\pi\cdots\pi$ stacking interactions between an electron rich uncoordinated azpy ligand and metal coordinated electron poor azpy ligands (see Figure 2).

On the other hand, there is no guest azpy molecule in the corresponding rectangular grid formed by Mn(2). But this grid stabilizes the uncoordinated azpy guest molecule in the grid of Mn(1) by host−guest hydrogen bonding interactions between the N(53) atom of bridging dicyanamide and H(33) of an azpy guest (dimensions of the hydrogen bond are C(33)···N(53)[a] 3.543 Å, C(33)−H(33)···N(53) 177°, and H···N 2.61 Å, symmetry code [a]: x, $-1+y$, z) as shown in Figure. 3.

Complex **2** features azpy ligand bridged 1D chains of centrosymmetric units $[Mn(NCS)_2(CH_3OH)_2]$ as shown in Figure 4 together with the atomic numbering scheme. In addition, there is a discrete azpy acting as an aromatic guest molecule.

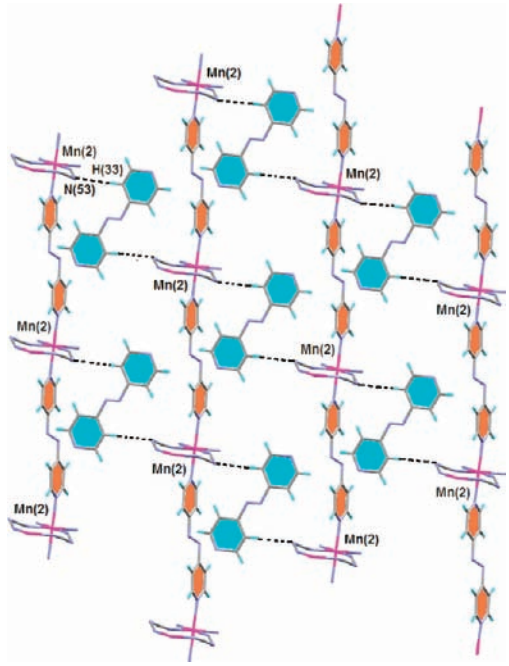

Figure 3. Formation of a 2D sheet involving hydrogen bonding interactions between azpy guests and nitrogen atoms of dicyanamide bridges.

Each six-coordinate octahedral Mn(II) center is bonded to two thiocyanate nitrogen atoms and two oxygen atoms from two methanol molecules in the basal plane and two azpy nitrogens at the axial sites. The bond lengths in the equatorial plane are 2.195(1) Å for Mn(1)−O(1) and 2.160(2)Å for Mn(1)−N(1), while the axial Mn(1)−N(11) distance is 2.312(2)Å. Selected bond lengths and angles are summarized in Table 3. The axially coordinated azpy ligands link the Mn(II) centers, yielding a 1D chain along the crystallographic c-axis. These chains assemble to form a grid framework by exploiting $CH_3\cdots\pi$ supramolecular interactions between the $-CH_3$ group of the coordinated methanol molecule of one chain with the pyridine ring of the bridging azpy of the neighboring chain (symmetry code: $-x-1$, $-y$, $-z$) in the a direction as shown in Figure 5.

dx.doi.org/10.1021/ic202129a | Inorg. Chem. 2012, 51, 1837−1851

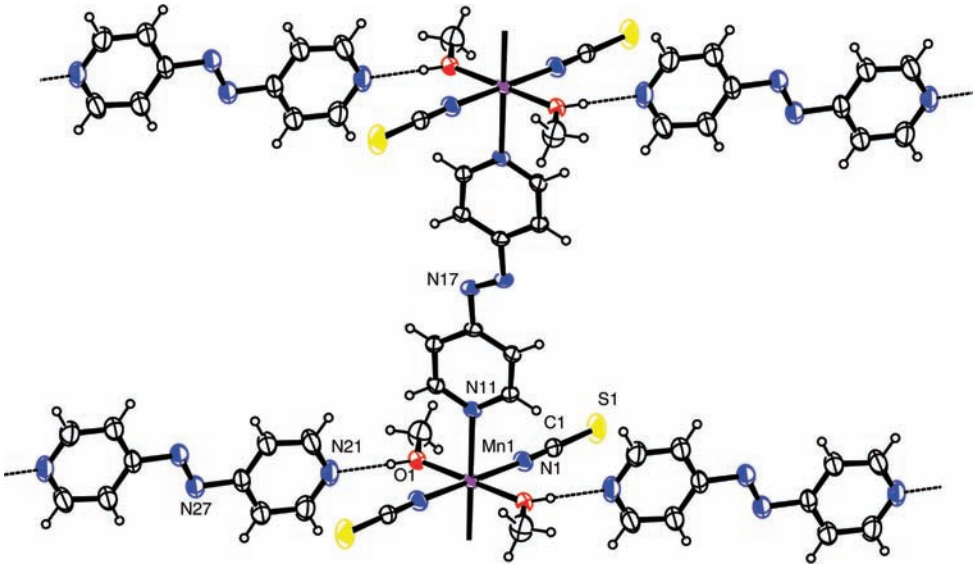

Figure 4. Structure of **2** with ellipsoids at 30% probability. Hydrogen bonds shown as dotted lines.

Table 3. Bond Distances (Å) and Angles (deg) in the Metal Coordination Spheres of Complex 2

atom labels	distance	atom labels	angle
Mn(1)−O(1)	2.195(2)	N(1)−Mn(1)−O(1)	93.22(7)
Mn(1)−N(1)	2.160(1)	N(1)−Mn(1)−N(11)	88.92(6)
Mn(1)−N(2)	2.312(2)	O(1)−Mn(1)−N(11)	89.94(6)

These grids further incorporate guest azpy molecules (Figure 6), with the help of a strong hydrogen bond between coordination-free nitrogen atom of the pyridine ring and methanolic −OH (dimensions of the hydrogen bond are H···N 1.87 Å, O−H···N 174°, and O···N 2.701(3) Å.) of two neighboring 1D chains in the *b* direction to form an overall 3D supramolecular structure.

The structure of **3** contains two metal atoms Mn(1) and Mn(2) in the asymmetric unit, and these are both in general positions as shown in Figures 7 and 8 together with the atom numbering scheme. Both independent manganese atoms are six-coordinate with slightly distorted octahedral environments.

Mn(1) is bonded to three oxygen atoms [O(1), O(2), O(3)] of water molecules and one pyridyl nitrogen [N(102)] of azpy ligand in the basal plane with one oxygen atom [O(4)] of a water molecule and a pyridyl nitrogen atom [N(31)] of another azpy ligand in axial positions completing the octahedral arrangement. Around Mn(1), bond lengths are Mn(1)−O(3) is 2.127(4) Å, Mn(1)−O(2) is 2.139(5) Å, Mn(1)−O(1) is 2.189(4) Å, Mn(1)−O(4) is 2.203(5) Å while Mn(1)−N(31) is 2.276(5) Å and Mn(1)−N(102) is 2.279(5) Å. It is interesting to note that there are two shorter Mn−O bonds, but these do not show any pattern in regard to trans atoms as one short O(2) and one long O(4) are both trans to coordinated nitrogens atom of pyridine rings.

By contrast, for Mn(2) four oxygen atoms [O(5), O(6), O(8), O(9)] of water molecules constitute the basal plane while one water molecule and one azpy nitrogen [N(62)] are coordinated axially. Distances around the metal are as follows; Mn(2)−O(5) 2.144(5) Å, Mn(2)−O(9) 2.149(5) Å, Mn(2)−O(6) 2.168(5) Å, Mn(2)−O(8) 2.178(6) Å, Mn(2)−O(7) 2.182(5) Å, and Mn(2)−N(62) 2.312(5) Å respectively. The root mean squared (r.m.s.) deviations of the four basal donor atoms from their mean planes around Mn(1) and Mn(2) are 0.095 and 0.027 Å, respectively. Selected bond lengths and angles are summarized in Table 4. The three azpy ligands associated with the two metal coordination spheres are not bridging. However all water molecules show the formation of

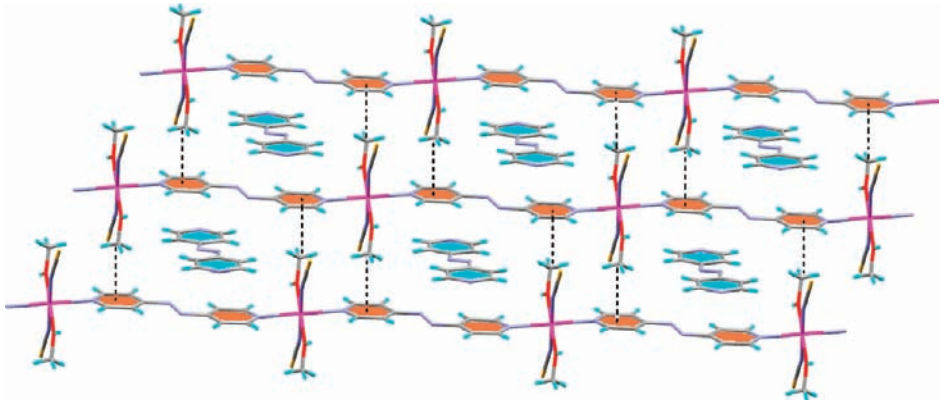

Figure 5. Formation of 2D host−guest complex involving $CH_3\cdots\pi$ interactions between coordinated methanols and azpy ligands of the neighboring chains.

dx.doi.org/10.1021/ic202129a | *Inorg. Chem.* 2012, 51, 1837−1851

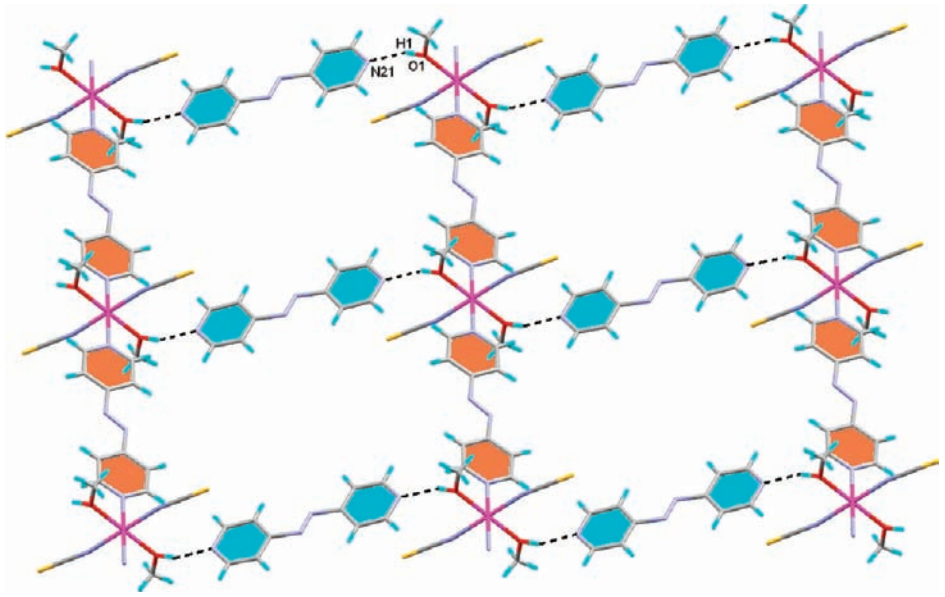

Figure 6. Host−guest hydrogen bonding interactions in **2** between coordinated methanol and guest azpy moieties.

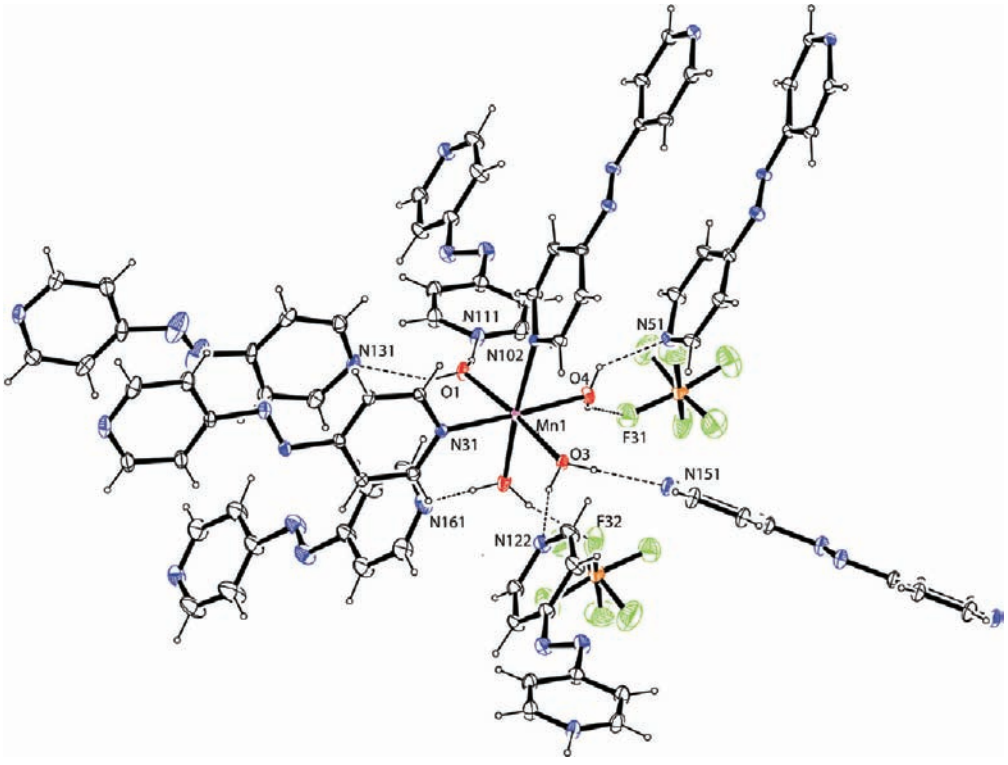

Figure 7. Arrangement around Mn(1) in **3** with ellipsoids at 10% probability. Hydrogen bonds shown as dotted lines.

hydrogen bonds primarily to associated azpy ligands to construct a 3D supramolecular framework (Supporting Information, Figure S7) details of which are given in Supporting Information, Table ST1. There are four additional azpy ligands in general positions and three more in which there is a center of symmetry at the midpoint of the central N−N bond.

In this compound there is an anion···π interaction between a hexafluorophosphate anion and the electron deficient metal (Mn1) coordinated heterocyclic azpy ring (Figure 9). At the same time the electron poor coordinated and uncoordinated azpy rings are further stabilized by π···π interactions, all of which contribute to the stabilization of the 3D supramolecular framework as discussed in the theoretical section.

Theoretical Studies. We have used the M06/6-31+G* level of theory because it is a good compromise between the size of the systems and the accuracy of the results. The M06 functional has been validated for both transition metal complexes and noncovalent interactions[21] and therefore it is highly recommended for applications in organometallic and coordination chemistry and for noncovalent interactions.[21] We have imposed the high spin configuration (five unpaired electrons) on the Mn ions and no spin contamination was generated in the calculations. With reference to the structure of

dx.doi.org/10.1021/ic202129a | *Inorg. Chem.* 2012, 51, 1837−1851

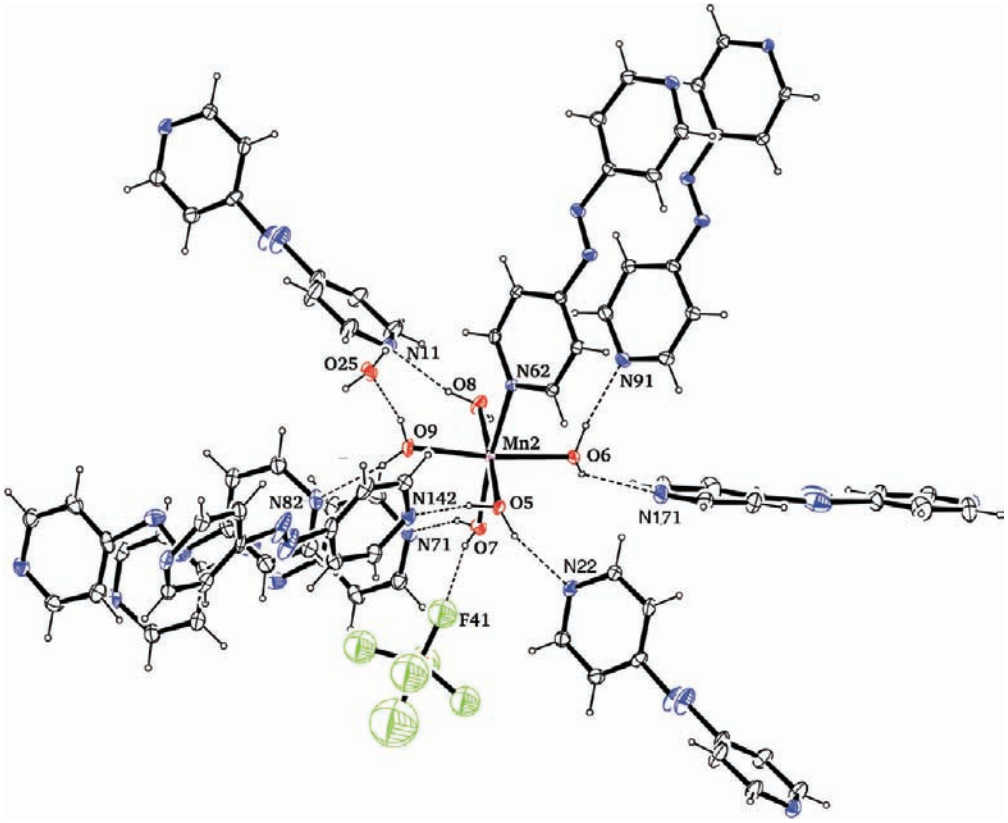

Figure 8. Arrangement around Mn(2) in **3** with ellipsoids at 10% probability. Hydrogen bonds shown as dotted lines.

Table 4. Bond Distances (Å) and Angles (deg) in the Metal Coordination Spheres of Complex 3

atom labels	distance or angle	atom labels	angle
Mn(1)−O(1)	2.189(4)	Mn(2)−O(5)	2.144(5)
Mn(1)−O(2)	2.139(5)	Mn(2)−O(9)	2.149(5)
Mn(1)−O(3)	2.127(4)	Mn(2)−O(6)	2.168(5)
Mn(1)−O(4)	2.203(5)	Mn(2)−O(8)	2.178(6)
Mn(1)−N(31)	2.276(5)	Mn(2)−O(7)	2.182(5)
Mn(1)−N(102)	2.279(5)	Mn(2)−N(62)	2.312(5)
O(3)−Mn(1)−O(2)	88.7(2)	O(5)−Mn(2)−O(9)	90.6(2)
O(3)−Mn(1)−O(1)	175.2(2)	O(5)−Mn(2)−O(6)	95.8(2)
O(2)−Mn(1)−O(1)	87.5(2)	O(9)−Mn(2)−O(6)	172.9(2)
O(3)−Mn(1)−O(4)	87.8(2)	O(5)−Mn(2)−O(8)	177.3(2)
O(2)−Mn(1)−O(4)	89.4(2)	O(9)−Mn(2)−O(8)	86.7(2)
O(1)−Mn(1)−O(4)	95.1(2)	O(6)−Mn(2)−O(8)	86.8(2)
O(3)−Mn(1)−N(31)	92.4(2)	O(5)−Mn(20)−O(7)	88.1(2)
O(2)−Mn(1)−N(31)	93.7(2)	O(9)−Mn(2)−O(7)	93.0(2)
O(1)−Mn(1)−N(31)	84.9(2)	O(6)−Mn(2)−O(7)	90.3(2)
O(4)−Mn(1)−N(31)	177.0(2)	O(8)−Mn(2)−O(7)	92.2(2)
O(3)−Mn(1)−N(102)	92.5(2)	O(5)−Mn(2)−N(62)	89.3(2)
O(2)−Mn(1)−N(102)	172.6(2)	O(9)−Mn(2)−N(62)	92.0(2)
O(1)−Mn(1)−N(102)	91.6(2)	O(6)−Mn(2)−N(62)	85.1(2)
O(4)−Mn(1)−N(102)	83.4(2)	O(8)−Mn(2)−N(62)	90.7(2)
N(31)−Mn(1)−N(102)	93.5(2)	O(7)−Mn(2)−N(62)	174.4(2)

complex **1**, we first evaluated the influence of the manganese coordination on the $\pi\cdots\pi$ stacking interaction. In Figure 10 we show the $\pi\cdots\pi$ interaction energies computed for the stacking between two azpy ligands. The 1:1 complex has ΔE_1 of −5.87 kcal/mol compared to constituent ligands. The interaction energy of the sandwich complex (2:1) is −13.86 kcal/mol, which is higher in absolute value than twice the ΔE_1 reported above indicating some cooperativity effects.

The influence of the coordination of manganese has been evaluated using the equations shown in Figure 11. We have used a theoretical model in which the manganese is coordinated to two azide (as models of $(CN)_2N^-$) ions to counterbalance the positive charge and to keep the model neutral, the other available coordination sites have been occupied by ammonia to reduce the size of the system. When one nitrogen atom of the ligand is coordinated to Mn(II) the stacking interaction is

dx.doi.org/10.1021/ic202129a | *Inorg. Chem.* 2012, 51, 1837−1851

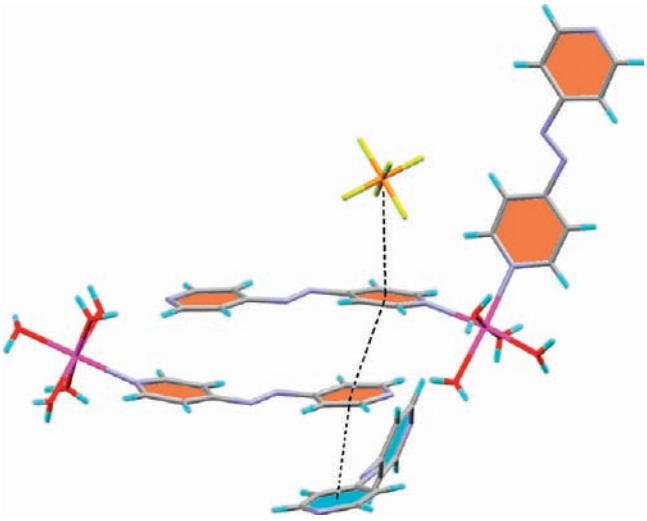

Figure 9. Anion···π and π···π interactions in complex **3**.

enhanced from −5.87 to −6.36 kcal/mol, indicating that the strength of the π···π interaction increases upon coordination. If the ligand is doubly coordinated to two Mn(II) ions, the stacking interaction further reinforces to −6.72 kcal/mol. Therefore in the crystal structure the π···π interaction is strong and very stabilizing because one azpy ligand is electron poor as a consequence of Mn coordination, thus favoring the π···π interaction.

We further studied the interaction of the ligand in a cage model that resembles the real situation observed in the crystal structure (Figure. 12). The affinity of this cage for the ligand is very high, since the interaction energy is ΔE_5 = −13.24 kcal/mol. This energy is approximately twice the value of ΔE_4, indicating that the model used above to evaluate the stacking between a coordinated azpy ligand with an uncoordinated one is adequate. This high interaction energy inside the cavity prevents any inside−outside movement of the intercalated guest. We have studied the possibility of rotation inside the cavity, and the barrier to rotating the guest around the main symmetry axis is 7.96 kcal/mol. A close examination of the host−guest complex reveals that one hydrogen atom of each pyridine moiety of the azpy guest is directed to the center of the lateral walls of the host. A favorable noncovalent interaction may be established between this hydrogen atom and the bridge $C_2N_3^-$ ligands that form the wall. To explore this possibility we have carried out additional calculations of a model (Figure 13) in which the azpy walls of the cage have been removed and only the walls formed by the bridging $C_2N_3^-$ ligands are conserved. The interaction energy is small (−0.95 kcal/mol) indicating that this interaction contributes only modestly to the binding.

With reference to the structure of **2** we have studied several aspects related to the relevant noncovalent interactions that are observed in the solid state. The stacking between both azpy moieties is very different from that observed for compound **1**. Therefore it is interesting to compare the energetic features of both orientations. In Figure 14 we show the interaction energies for the double and triple-decker complexes. The interaction energy of the π···π stacking (in the absence of Mn) in compound **2** is 0.51 kcal/mol less favorable than that calculated for the stacking in compound **1**.

In this complex, a small cooperativity between both π···π interactions is also observed.

The influence of the coordination of one azpy ligand to two Mn(II) ions is shown in Figure 15. As can be observed the influence on the stacking is significant since the interaction energy becomes almost 3 kcal/mol more favorable. The most important feature in this compound is that the host cavity is formed by a self-assembly of two coordinated ligands by means of two CH_3···π interactions (Figure. 15, bottom). This self-assembly is energetically favored because the acidity of the hydrogen atoms of the methyl group is enhanced by the presence of the Mn(II) ion coordinated to the adjacent oxygen atom. The interaction energy of each CH_3···π interaction is estimated to be −3.67 kcal/mol ($\Delta E_{10}/2$). The importance of this interaction should be emphasized, since it is responsible for the self-assembly of two Mn complexes that generates the cavity. These results demonstrate that the interaction is energetically very favorable, especially if compared to standard C−H/π interactions, which are weak (∼1 kcal/mol).[25] In addition, experimental results mentioned above confirm the key role of this interaction, since the solid isolated after removal of its guest by heating reverts to compound **2** on crystallization from methanol but transforms into $\{[Mn(NCS)_2(azpy)_2]\text{-azpy}\}_n$, on crystallization from ethanol. Therefore it is clear that

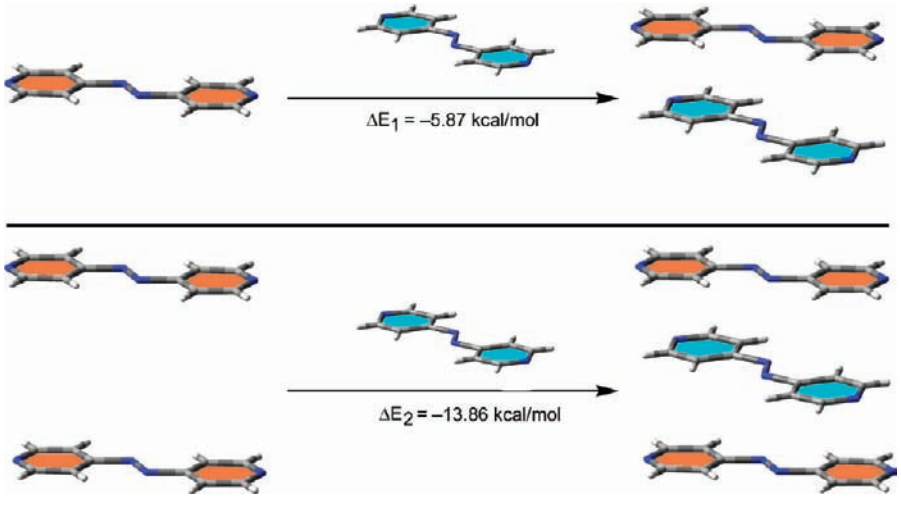

Figure 10. Theoretical analysis of the stacking energy for compound **1**.

dx.doi.org/10.1021/ic202129a | *Inorg. Chem.* 2012, 51, 1837−1851

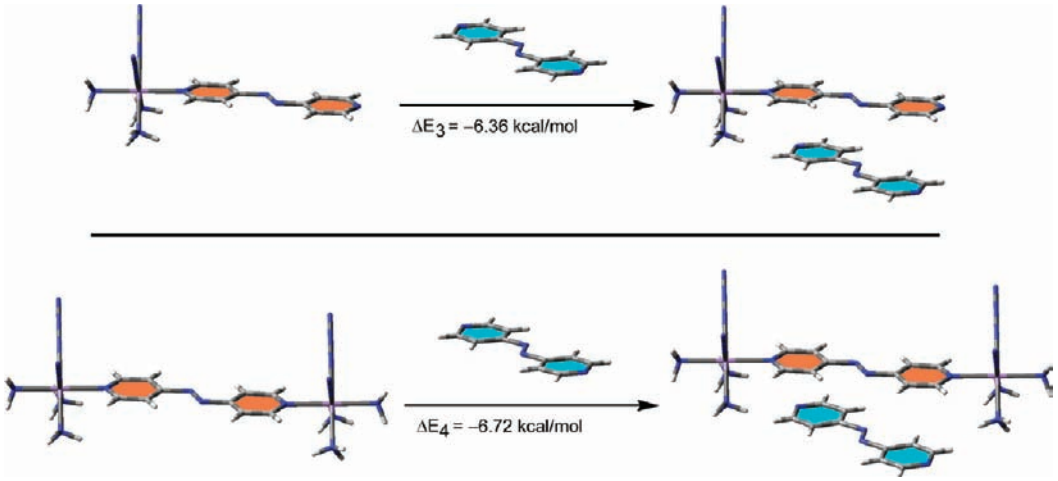

Figure 11. Theoretical analysis of the effect of Mn on the stacking interaction in compound **1**.

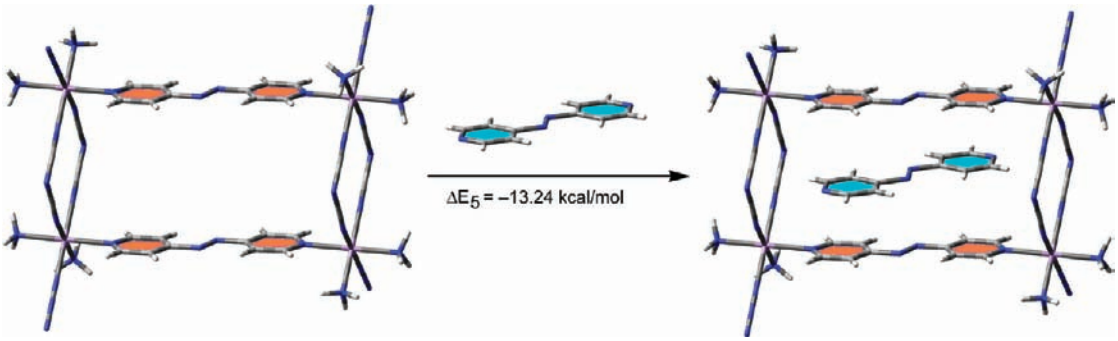

Figure 12. Host–guest complex and its associated interaction energy in **1**.

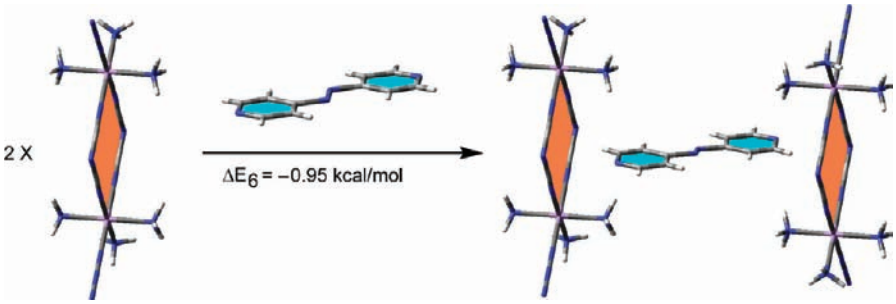

Figure 13. Interaction energy of the ligand with the walls.

the presence of the methanol molecule and the occurrence of $CH_3\cdots\pi$ interactions play a decisive role in the self-assembly and 3D architecture of **2**.

The orientation of the azpy guest in the complex in compound **2** is clearly dominated by the two H-bonds that are formed between pyridine nitrogen atoms in azpy and the methanol molecules coordinated to the Mn ion. In this theoretical study we have also examined the influence of the Mn on the strength of the H-bonding. The equations shown in Figure. 16 allow us to evaluate this effect. It can be observed that each hydrogen bonding interaction accounts for −3.02 kcal/mol in the absence of Mn(II). The H-bonding interaction considerably strengthens to −8.60 kcal/mol when the MeOH hydrogen bonding donor is coordinated to Mn(II) as a consequence of the increase in the acidity of the MeOH proton.

Finally, we have computed the interaction energy of the self-assembled cage with the ligand, as illustrated in Figure 17. The interaction energy is ΔE_{13} = −17.82 kcal/mol, which is even higher than the interaction energy computed for compound **1**. In addition, if we compare this energy (ΔE_{13}) with ΔE_9 = −8.16 kcal/mol, where only one stacking interaction is present, the ΔE_{13} value is more than twice the ΔE_9 value, indicating that the stacking interaction in the cage is enhanced by the presence of the $CH_3\cdots\pi$ interactions. It should be mentioned that the stacking interactions in these systems are especially favorable because one π-system is poor because of the effect of the Mn coordination and the other is rich. The $CH_3\cdots\pi$ interaction further increases the π-acidity of the neighboring ring, thus favoring the $\pi\cdots\pi$ stacking interaction.

For structure **3** we have studied theoretically an interesting anion$\cdots\pi$ interaction that is established between a PF_6^- anion and one azpy ligand coordinated to a Mn(II) ion. This moiety

dx.doi.org/10.1021/ic202129a | *Inorg. Chem.* 2012, 51, 1837–1851

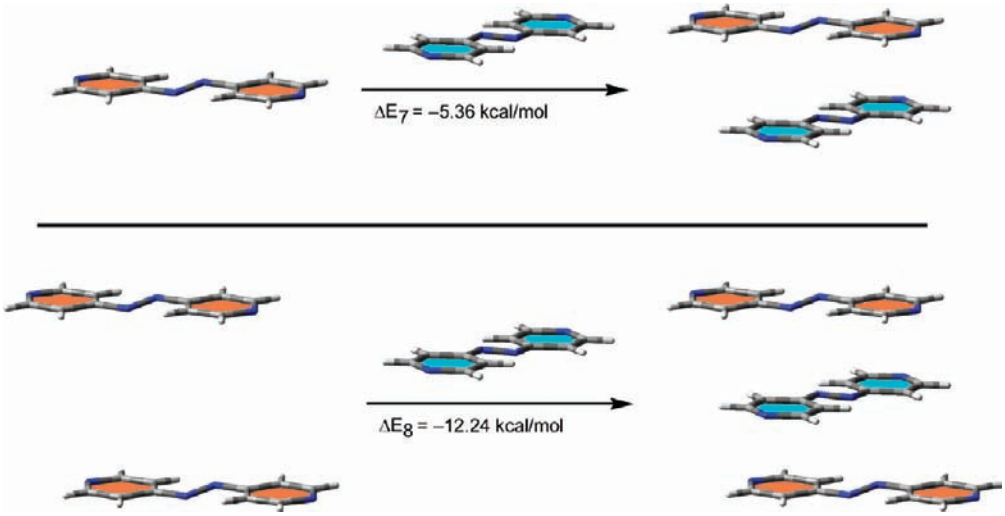

Figure 14. Theoretical analysis of the stacking energy for compound **2**.

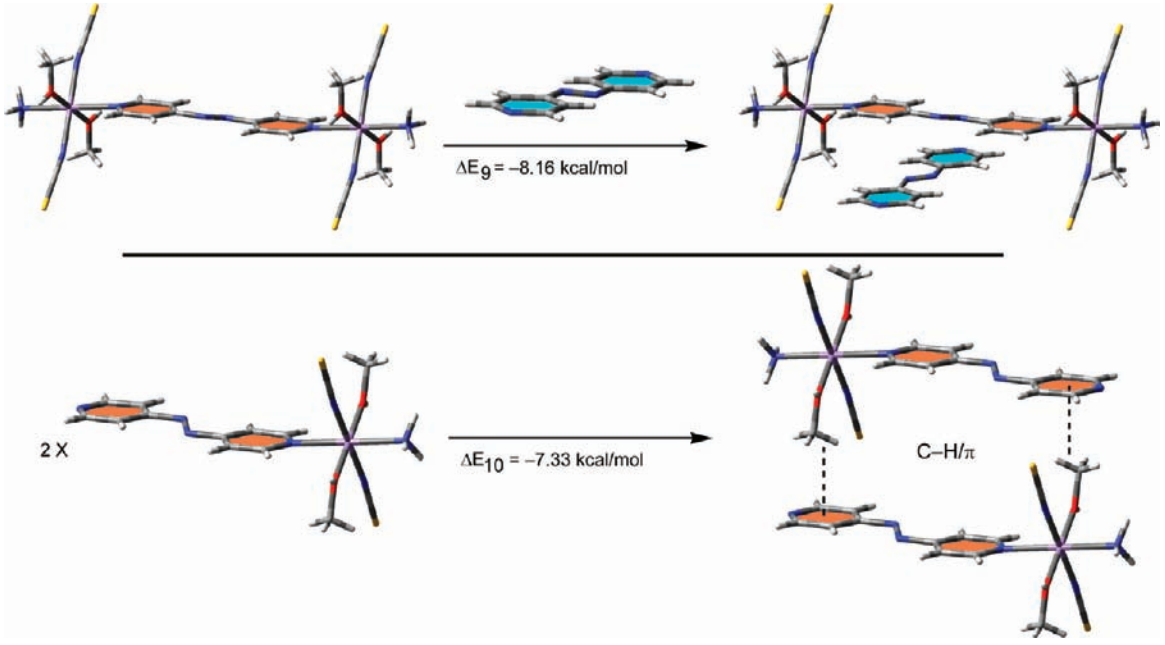

Figure 15. Top: Theoretical analysis of the effect of Mn on the stacking interaction in compound **2**. Bottom: Self-assembly to generate the supramolecular cage in **2**.

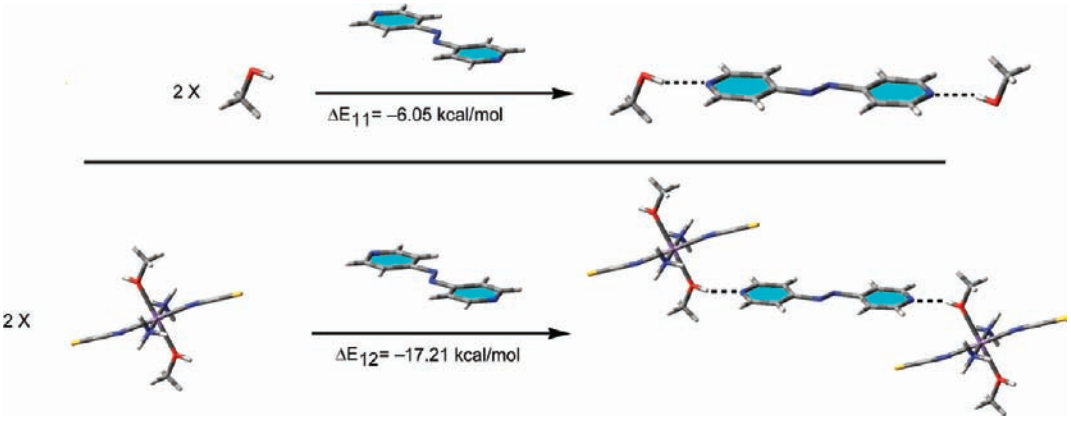

Figure 16. Effect of Mn(II) coordination on the H-bonding energy.

dx.doi.org/10.1021/ic202129a | *Inorg. Chem.* 2012, 51, 1837–1851

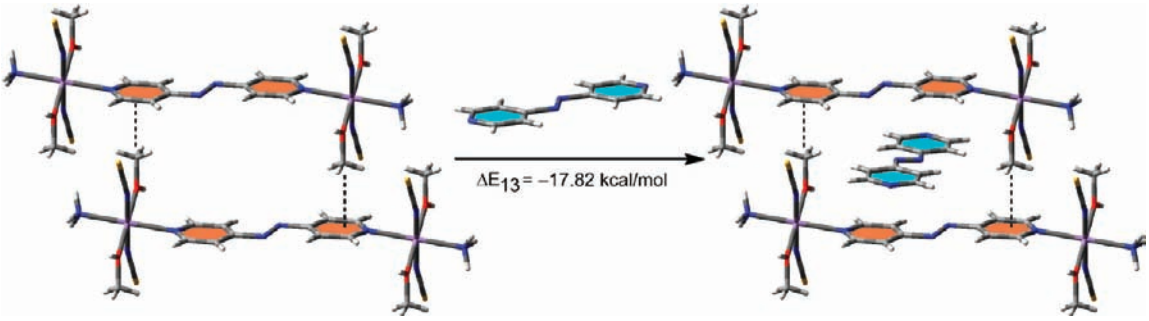

Figure 17. Host−guest complex and its associated interaction energy in **2**.

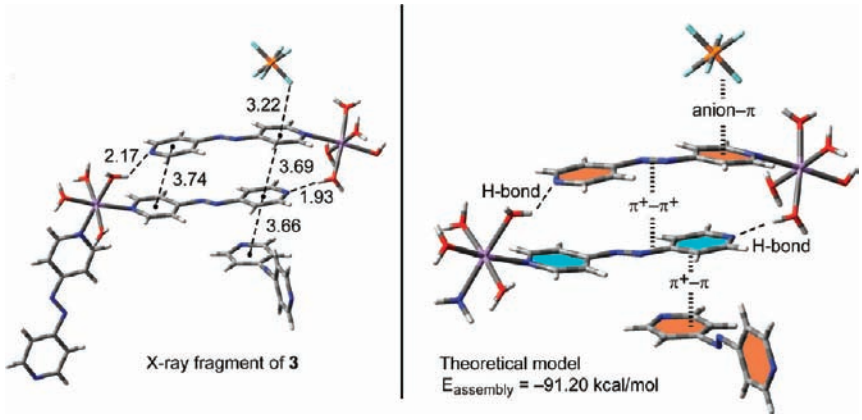

Figure 18. Crystal fragment exhibiting the anion−$\pi/\pi^+-\pi^+/\pi^+-\pi$ assembly and the theoretical model. Distances in Å.

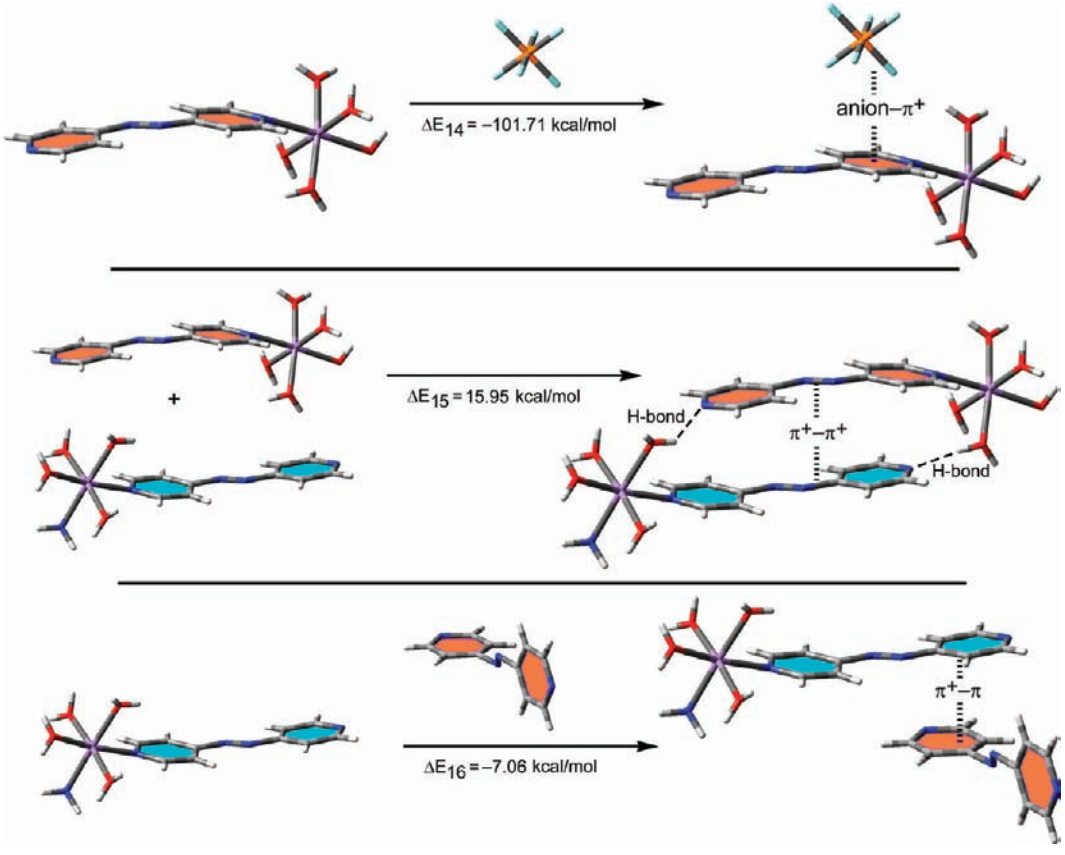

Figure 19. Equations used to compute the interaction energies of the three parts that constitute the assembly, part of **3**.

dx.doi.org/10.1021/ic202129a | *Inorg. Chem.* 2012, 51, 1837−1851

has a global charge of +2 and therefore it is able to interact strongly with anions because of electrostatic effects. To differentiate this positively charged fragment from the neutral, we have denoted the π system that it is bonded to a charged Mn atom as π^+. An interesting issue is that this moiety is able to form a $\pi-\pi$ stacking (denoted as $\pi^+-\pi^+$ interaction) with a similar one. In principle, this should be very unfavorable because the charge repulsion should be high. Since both anion$-\pi$ and $\pi^+-\pi^+$ interaction coexist, we have analyzed how they influence the formation energy of the assembly. In Figure 18 we show the fragment of the crystal structure that forms the supramolecular anion$-\pi/\pi^+-\pi^+/\pi^+-\pi$ assembly, which is analyzed in the present theoretical study. In the theoretical model one azpy ligand has been replaced by ammonia to reduce the size of the system.

First of all we evaluated the formation energy of the whole assembly shown in Figure 18 with respect to the isolated monomers. Keeping in mind that the two middle moieties, $[Mn(azpy)(OH_2)_4(NH_3)]^+$ and $[Mn(azpy)(OH_2)_5]^+$, of the assembly are both positively charged, then the formation energy is unexpectedly very favorable (−91.2 kcal/mol), indicating that this assembly is a strong binding motif in the crystal structure. We have also evaluated the formation energy of the different binary systems that constitute the assembly to understand this strong binding energy. The equations used to evaluate the interaction energies are indicated in Figure 19.

Very interesting conclusions can be extracted from the energies gathered in Figure. 19. First, the anion$-\pi^+$ interaction is very favorable. This is due to the proximity of the doubly positive charged Mn atom, which provokes a dual effect, favoring both the interaction due to pure electrostatic attraction and its coordination to the azpy ligand which considerably increases the π-acidity of the pyridine ring, as previously demonstrated for other transition metals coordinated to pyridine.[26] In fact the anion$-\pi^+$ distance is very short (3.22 Å) for the PF_6^- anion in comparison with other structures.[27] Second, ΔE_{15} is surprisingly small, taking into account that each interacting part has two positive charges and, consequently, a strong electrostatic repulsion is expected. A likely explanation is that two strong hydrogen bonds contribute to the stabilization of this binary complex and to some extent offset this repulsion. Furthermore, the more positively charged regions are located at the two Mn ions, which are distant from each other. In addition the stacking interaction is formed in such a way that the most π-acidic pyridine ring (the one coordinated to Mn) of one azpy ligand is stacked above the electron rich pyridine of the other azpy ligand and vice versa. Finally, the third interaction ($\pi^+-\pi$ stacking) is favorable (−7.06 kcal/mol) contributing to the global stabilization of the system. This interaction energy is in agreement with similar systems reported in the literature where the stacking interaction is established between a neutral electron rich π-system and a positively charged aromatic ring.[28] Examining the interaction energies of the binary systems shown in Figure 19, it is clear that the supramolecular anion$-\pi/\pi^+-\pi^+/\pi^+-$ assembly is stabilized mainly because of the anion$-\pi$ interaction and, to a lesser extent, by the $\pi^+-\pi$ interaction. In solution, the favorable interaction between positively charged moieties has been studied. For instance, Piguet et al.[29] have demonstrated that solvation is the origin of the surprising stabilities of highly charged self-assembled polymetallic complexes.

CONCLUSIONS

Three new manganese(II) coordination compounds have been synthesized using the primary ligands, dicyanamide, thiocyanate, and hexafluorophosphate, respectively, together with azpy as the secondary spacer. All three complexes have been characterized by single crystal X-ray crystallography and thermal analyses. The final molecular structures of the self-assembled species are very different. Complex **1** forms a 2D grid sheet motif that assembles to form a microporous framework that incorporates coordination-free azpy by several nonbonding interactions. Complex **2** features azpy ligand bridged 1D chains of centrosymmtric units $[Mn(NCS)_2(CH_3OH)_2]$ which, by means of a very interesting and crucial $CH_3-\pi$ supramolecular interaction, forms a 2D porous sheet. A guest azpy molecule is incorporated within the pores by strong H-bonding interactions. Complex **3** affords a 0-D motif with two monomeric Mn(II) units in general positions in the asymmetric unit, which are joined together by H-bonds, anion$-\pi/\pi^+-\pi^+/\pi^+-\pi$ interactions. The investigation herein reported also reflects that a complete prediction of the self-assembly of crystalline materials is obviously still not possible. Indeed, a mere change in solvent conditions or counterions can bring dramatic structural changes in the solid-state packing of molecules.

The theoretical part provides an energetic study of the noncovalent interactions that are responsible for the supramolecular assemblies observed in the solid state. It nicely complements the experimental (structural and thermal analyses) results, emphasizing the importance of the noncovalent interactions and their interplay in the solid-state structures of the compounds explored. In addition, we have analyzed the influence of the Mn ion on several noncovalent interactions (H-bonding, $\pi-\pi$ stacking and $CH_3-\pi$). We have provided an energetic partition study of the individual noncovalent interactions that are responsible of the supramolecular assemblies observed in the solid state. It demonstrates the existence of interesting cooperativity effects between the noncovalent interactions, and it is useful to understand the formation of the anion$-\pi/\pi^+-\pi^+/\pi^+-\pi$ assembly found in compound **3**.

ASSOCIATED CONTENT

Supporting Information

TG curve of complexes **1** and **2**, the XRD patterns of complexes **1** and **2**, TG curve of complex **3**, the coordination environment around Mn(2) in complex**1**, formation of the 3D supramolecular framework of complex **3** are represented in Figures S1, S2, S3, S4, S5, S6, and S7 respectively, hydrogen bond geometries in **3** are presented in Table-ST1, and Crystallographic data in CIF format for the structures reported. This material is available free of charge via the Internet at http://pubs.acs.org.

AUTHOR INFORMATION

Corresponding Author

*E-mail: toni.frontera@uib.es (A.F.), ghosh_59@yahoo.com (A.G.).

ACKNOWLEDGMENTS

P.K. and R.B. are thankful to CSIR, India, for research fellowships [Sanction no. 09/028(0733)/2008-EMR-I and 09/028(0746)/2009-EMR-I]. We thank EPSRC and the University

of Reading for funds for the X-Calibur CCD Diffractometer and the DST-FIST, India-funded Single Crystal Diffractometer Facility at the Department of Chemistry, University of Calcutta, for the Bruker-Smart Diffractometer. A.F. thanks CONSOLIDER–Ingenio 2010 (CSD2010-0065) and the MICINN of Spain (project CTQ2008-00841/BQU, FEDER funds) for financial support and the CESCA for computational facilities. Assistance from Carolina Estarellas at the early stage of this work is acknowledged.

REFERENCES

(1) (a) Teo, P.; Hor, T. S. A. *Coord. Chem. Rev.* **2011**, *255*, 273–289. (b) Qiu, S.; Zhu, G. *Coord. Chem. Rev.* **2009**, *253*, 2891–2911. (c) Suh, M. P.; Cheon, Y. E.; Lee, E. Y. *Coord. Chem. Rev.* **2008**, *252*, 1007–1026. (d) Zhao, X.; He, H.; Hu, T.; Dai, F.; Sun, D. *Inorg. Chem.* **2009**, *48*, 8057–8059. (e) Biswas, C.; Mukherjee, P.; Drew, M. G. B.; Gomez-Garcia, C. J.; Clemente-Juan, J. M.; Ghosh, A. *Inorg. Chem.* **2007**, *46*, 10771–10780.

(2) (a) Nagaoka, M.; Ohta, Y.; Hitomi, H. *Coord. Chem. Rev.* **2007**, *251*, 2522–2536. (b) Ma, M.; Zacher, D.; Zhang, X.; Fischer, R. A.; Metzler-Nolte, N. *Cryst. Growth Des.* **2011**, *11*, 185–189. (c) Eubank, J. F.; Mouttaki, H.; Cairns, A. J.; Belmabkhout, Y.; Wojtas, L.; Luebke, R.; Alkordi, M.; Eddaoudi, M. *J. Am. Chem. Soc.* **2011**, *133* (36), 14204–14207. (d) Biswas, C.; Drew, M. G. B.; Ghosh, A. *Inorg. Chem.* **2008**, *47*, 4513–4519.

(3) (a) Sun, D.; Ma, S.; Ke, Y.; Collins, D. J.; Zhou, H.-C. *J. Am. Chem. Soc.* **2006**, *128*, 3896–3897. (b) Atci, E.; Erucar, I.; Keskin, S. *J. Phys. Chem. C* **2011**, *115*, 6833–6840. (c) Klontzas, E.; Mavrandonakis, A.; Tylianakis, E.; Froudakis, G. E. *Nano Lett.* **2008**, *8*, 1572–1576.

(4) (a) Hamon, L.; Llewellyn, P. L.; Devic, T.; Ghoufi, A.; Clet, G.; Guillerm, V.; Pirngruber, G. D.; Maurin, G.; Serre, C.; Driver, G.; Beek, W. v.; Jolimatre, E.; Vimont, A.; Daturi, M.; Frey, G. *J. Am. Chem. Soc.* **2009**, *131*, 17490–17499. (b) Duan, L.; Wu, Z.-H.; Ma, J.-P.; Wu, X.-W.; Dong, Y.-B. *Inorg. Chem.* **2010**, *49*, 11164–11173. (c) Hu, J.; Cai, H.; Ren, H.; Wei, Y.; Xu, Z.; Liu, H.; Hu, Y. *Ind. Eng. Chem. Res.* **2010**, *49*, 12605–12612. (d) Li, J.-R.; Ma, Y.; McCarthy, M. C.; Sculley, J.; Yu, J.; Jeong, H.-K.; Balbuena, P. B.; Zhou, H.-C. *Coord. Chem. Rev.* **2011**, *255*, 1791–1823.

(5) (a) Shultz, A. M.; Farha, O. K.; Hupp, J. T.; Nguyen, S. T. *J. Am. Chem. Soc.* **2009**, *131*, 4204–4205. (b) Gándara, F.; Gomez-Lor, B.; Gutiérrez-Puebla, E.; Iglesias, M.; Monge, M. A.; Proserpio, D. M.; Snejko, N. *Chem. Mater.* **2008**, *20*, 72–76.

(6) (a) Gándara, F.; Andrés, A. d.; Gómez-Lor, B.; Gutiérrez-Puebla, E.; Iglesias, M.; Monge, M. A.; Proserpio, D. M.; Snejko, N. *Cryst. Growth Des.* **2008**, *8*, 378–380. (b) Martínez, C.; Corma, A. *Coord. Chem. Rev.* **2011**, *255*, 1558–1580. (c) Atwood, J. D. *Coord. Chem. Rev.* **1988**, *83*, 93–114.

(7) (a) Alaerts, L.; Seguin, E.; Poelman, H.; Thibault-Starzyk, F.; Jacobs, P. A.; Vos, D. E. D. *Chem.—Eur. J.* **2006**, *12*, 7353–7363. (b) Ma, L.; Abney, C.; Lin, W. *Chem. Soc. Rev.* **2009**, *38*, 1248–1256. (c) Lee, J.; Farha, O. K.; Roberts, J.; Scheidt, K. A.; Nguyen, S. T.; Hupp, J. T. *Chem. Soc. Rev.* **2009**, *38*, 1450–1459.

(8) (a) Gomez-Lor, B.; Gutierrez-Puebla, E.; Iglesias, M.; Monge, M. A.; Ruiz-Valero, C.; Snejko, N. *Chem. Mater.* **2005**, *17*, 2568–2573. (b) Hwang, Y. K.; Hong, D.-Y.; Chang, J.-S.; Jhung, S. H.; Seo, Y.-K.; Kim, J.; Vimont, A.; Daturi, M.; Serre, C.; Ferey, G. *Angew. Chem., Int. Ed.* **2008**, *47*, 4144–4148.

(9) (a) Yu, R.; Kuang, X.-F.; Wu, X.-Y.; Lu, C.-Z.; Donahue, J. P. *Coord. Chem. Rev.* **2009**, *253*, 2872–2890. (b) Zhang, Y.; Gu, H.; Yang, Z.; Xu, B. *J. Am. Chem. Soc.* **2003**, *125*, 13680–13681. (c) Fuss, M.; Luna, M.; Alcantara, D.; de la Fuente, J. M.; Enríquez- Navas, P. M.; Angulo, J.; Penads, S.; Briones, F. *J. Phys. Chem. B* **2008**, *112*, 11595–11600.

(10) (a) Maji, T. K.; Mostafa, G.; Matsuda, R.; Kitagawa, S. *J. Am. Chem. Soc.* **2005**, *127*, 17152–17153. (b) Dey, R.; Haldar, R.; Maji, T. K.; Ghoshal, D. *Cryst. Growth Des.* **2011**, *11* (9), 3905–3911. (c) Gurunatha, K. L.; Mohapatra, S.; Suchetan, P. A.; Maji, T. K. *Cryst. Growth Des.* **2009**, *9*, 3844–3847.

(11) (a) Kitagawa, S.; Uemura, K. *Chem. Soc. Rev.* **2005**, *34*, 109–119. (b) Kumagai, H.; Arishima, M.; Kitagawa, S.; Ymada.; Kawata, S.; Kaizaki, S. *Inorg. Chem.* **2002**, *41*, 1989–1992.

(12) (a) de Lill, D. T.; Cahill, C. L. *Cryst. Growth Des.* **2007**, *7*, 2390–2393. (b) Hazra, S.; Sarkar, B.; Naiya, S.; Drew, M. G. B.; Frontera, A.; Escudero, D.; Ghosh, A. *Cryst. Growth Des.* **2010**, *10*, 1677–1687. (c) Manimaran, B.; Lai, L.-J.; Thanasekaran, P.; Wu, J.-Y.; Liao, R.-T.; Tseng, T.-W.; Liu, Y.-H.; Lee, G.-H.; Peng, S.-M.; Lu, K.-L. *Inorg. Chem.* **2006**, *45*, 8070–8077. (d) Kar, P.; Biswas, R.; Ida, Y.; Ishida, T.; Ghosh, A. *Cryst. Growth Des.* **2011**, *11* (12), 5305–5315.

(13) (a) Ghosh, S. K.; Ribas, J.; Bharadwaj, P. K. *Cryst. Growth Des.* **2005**, *5*, 623–629. (b) Wang, C.-C.; Yang, C.-C.; Yeh, C.-T.; Cheng, K.-Y.; Chang, P.-C.; Ho, M.-L.; Lee, G.-H.; Shih, W.-J.; Sheu, H.-S. *Inorg. Chem.* **2011**, *50*, 597–603. (c) Lewiński, J.; Zachara, J.; Justyniak, I.; Dranka, M. *Coord. Chem. Rev.* **2005**, *249*, 1185–1199.

(14) (a) Biswas, C.; Drew, M. G. B.; Escudero, D.; Frontera, A.; Ghosh, A. *Eur. J. Inorg. Chem.* **2009**, 2238–2246. (b) Robin, A. Y.; Fromm, K. M. *Coord. Chem. Rev.* **2006**, *250*, 2127–2157. (c) Bassani, D. M.; Jonusauskaite, L.; Lavie-Cambot, A.; McClenaghan, N. D.; Pozzo, J.-L.; Ray, D.; Vives, G. *Coord. Chem. Rev.* **2010**, *254*, 2429–2445. (d) Domasevitch, K. V.; Gural'skiy, I. A.; Solntsev, P. V.; Rusanov, E. B.; Krautscheid, H.; Howard, J. A. K.; Chernega, A. N. *Dalton Trans.* **2007**, 3140–3148. (e) Domasevitch, K. V.; Solntsev, P. V.; Gural'skiy, I. A.; Krautscheid, H.; Rusanov, E. B.; Chernega, A. N.; Howard, J. A. K. *Dalton Trans.* **2007**, 3893–3905.

(15) (a) Noro, S.-i.; Kitagawa, S.; Nakamura, T.; Wada, T. *Inorg. Chem.* **2005**, *44*, 3960–3971. (b) Noro, S.-i.; Kondo, M.; Ishii, T.; Kitagawa, S.; Matsuzaka, H. *J. Chem. Soc., Dalton Trans.* **1999**, 1569–1574. (c) Barrio, J. P.; Rebilly, J.-N.; Carter, B.; Bradshaw, D.; Bacsa, J.; Ganin, A. Y.; Park, H.; Trewin, A.; Vaidhyanathan, R.; Cooper, A. I.; Warren, J. E.; Rosseinsky, M. J. *Chem.—Eur. J.* **2008**, *14*, 4521–4532.

(16) Brown, E. V.; Granneman, G. R. *J. Am. Chem. Soc.* **1975**, *97*, 621–627.

(17) *SAINT*, version 6.02; Bruker AXS, Inc.: Madison, WI, 2002. *SADABS*, version 2.03; Bruker AXS, Inc.: Madison, WI, 2002.

(18) Sheldrick, G. M. *SHELXS 97, Program for Structure Solution*; University of Göttingen: Göttingen, Germany, 1997.

(19) Sheldrick, G. M. *SHELXL 97, Program for Crystal Structure Refinement*; University of Göttingen: Göttingen, Germany, 1997.

(20) Frisch, M. J.; Trucks, G. W.; Schlegel, H. B.; Scuseria, G. E.; Robb, M. A.; Cheeseman, J. R.; Scalmani, G.; Barone, V.; Mennucci, B.; Petersson, G. A.; Nakatsuji, H.; Caricato, M.; Li, X.; Hratchian, H. P.; Izmaylov, A. F.; Bloino, J.; Zheng, G.; Sonnenberg, J. L.; Hada, M.; Ehara, M.; Toyota, K.; Fukuda, R.; Hasegawa, J.; Ishida, M.; Nakajima, T.; Honda, Y.; Kitao, O.; Nakai, H.; Vreven, T.; Montgomery, Jr., J. A.; Peralta, J. E.; Ogliaro, F.; Bearpark, M.; Heyd, J. J.; Brothers, E.; Kudin, K. N.; Staroverov, V. N.; Kobayashi, R.; Normand, J.; Raghavachari, K.; Rendell, A.; Burant, J. C.; Iyengar, S. S.; Tomasi, J.; Cossi, M.; Rega, N.; Millam, N. J.; Klene, M.; Knox, J. E.; Cross, J. B.; Bakken, V.; Adamo, C.; Jaramillo, J.; Gomperts, R.; Stratmann, R. E.; Yazyev, O.; Austin, A. J.; Cammi, R.; Pomelli, C.; Ochterski, J. W.; Martin, R. L.; Morokuma, K.; Zakrzewski, V. G.; Voth, G. A.; Salvador, P.; Dannenberg, J. J.; Dapprich, S.; Daniels, A. D.; Farkas, Ö.; Foresman, J. B.; Ortiz, J. V.; Cioslowski, J.; Fox, D. J. *Gaussian 09*, Revision B.01; Gaussian, Inc.: Wallingford, CT, 2009.

(21) Truhlar, D. G.; Zhao, Y. *Theor. Chem. Acc.* **2006**, *120*, 215.

(22) Boys, S. F.; Bernardi, F. *Mol. Phys.* **1970**, *19*, 553.

(23) Zhua, L.-N.; Ou-Yang, Y.; Liu, Z.-Q.; Liao, D.-Z.; Jiang, Z.-H.; Yan, S.-P.; Cheng, P. *Z. Anorg. Allg. Chem.* **2005**, *631*, 1693–1697.

(24) Ray, A.; Pilet, G.; Gómez-García, C. J.; Mitra, S. *Polyhedron* **2009**, *28*, 511.

(25) Nishio, M.; Hirota, M.; Umezawa, Y. *The CH/π Interaction. Evidence, Nature and Consequences*; Wiley-VCH: New York, 1998.

(26) (a) Quiñonero, D.; Frontera, A.; Deyà, P. M. *ChemPhysChem* **2008**, *9*, 397. (b) Gural'skiy, I. A.; Escudero, D.; Frontera, A.; Solntsev, P. V.; Rusanov, E. B.; Chernega, A. N.; Krautscheid, H.; Domasevitch, K. V. *Dalton Trans.* **2009**, 2856.

(27) (a) Schottel, B. L.; Chifotides, H. T.; Shatruk, M.; Chouai, A.; Perez, L. M.; Bacsa, J.; Dunbar, K. R. *J. Am. Chem. Soc.* **2006**, *128*, 5895. (b) Black, C. A.; Hanton, L. R.; Spicer, M. D. *Chem. Commun.* **2007**, 3171. (c) Frontera, A.; Gamez, P.; Mascal, M.; Mooibroek, T. J.; Reedijk, J. *Angew. Chem., Int. Ed.* **2011**, *50*, 9564.
(28) Geronimo, I.; Singh, N. J.; Kim, K. S. *Phys. Chem. Chem. Phys.* **2011**, *13*, 11841.
(29) Canard, G.; Piguet, C. *Inorg. Chem.* **2007**, *46*, 3511; and references cited therein.